Title:

Large-scale cortical synchronization promotes multisensory processing: An EEG study of visual-tactile pattern matching

Peng Wang[a,*,1], Florian Göschl[a,*,1], Uwe Friese[a], Peter König[a,b], and Andreas K. Engel[a]

[1] These authors contributed equally.

[a] Department of Neurophysiology and Pathophysiology, University Medical Center Hamburg-Eppendorf, Martinistr. 52, 20246 Hamburg, Germany

[b] Institute of Cognitive Science, University of Osnabrück, Albrechtstr. 28, 49069 Osnabrück

[*] *Correspondence address:*

Peng Wang, Phone: 0049-40-741052622, E-mail: p.wang@uke.de

Florian Göschl, Phone: 0049-40-741057476, E-mail: f.goeschl@uke.de

Department of Neurophysiology and Pathophysiology, University Medical Center Hamburg-Eppendorf, Martinistr. 52, 20246 Hamburg, Germany.

Keywords:

multisensory, cortical oscillations, coherence, coupling, EEG, beta-band, long-range synchrony

Abstract

The integration of sensory signals from different modalities requires flexible interaction of remote brain areas. One candidate mechanism to establish local and long-range communication in the brain is transient synchronization of neural assemblies. In addition to the analysis of oscillatory power, assessment of the phase dynamics of multiple brain signals is a promising avenue to examine the integration of distributed information in multisensory networks.

In the current study, human participants were engaged in a visual-tactile pattern matching task while high-density electroencephalograms (EEG) were recorded. To investigate the neural correlates of multisensory integration and assess effects of crossmodal stimulus congruence, we adapted an approach for purely data-driven analysis of neuronal coupling in source space that has recently been developed within our group. This method allows imaging of large-scale cortical networks in space, time and frequency without defining a priori constraints.

We identified three clusters of interacting sources that synchronized in the beta-band (~ 20 Hz). The spatial and spectro-temporal profile of the first two clusters suggest an involvement in crossmodal sensory processing, whereas the third cluster appears to reflect decision-related processes. By directly relating coupling features to task performance, we demonstrate that the phase of neural coherence within the observed networks predicts behavior. Our results provide further evidence that neural synchronization is crucial for long-range communication in the brain and suggest a possible role of beta-band activity in multisensory integration.

Significance Statement

The natural environment is rich of information, which is sampled by the different sensory organs, and further perceived as light, sound, smell, taste and touch etc. Despite being processed by spatially distinct brain areas, rather than remaining isolated features, they ultimately form a unified, coherent percept. How this integration is organized on the cortical level remains poorly understood. In this study, we asked participants to detect pre-defined target patterns in visual-tactile stimulus combinations while high-density electroencephalograms were recorded. Without a priori assumptions, we identified several networks across remote brain areas, which are responsible for multisensory perception and sensorimotor integration. Synchronization within the observed networks occurred in the beta-band (~ 20 Hz). Phase relations of these interactions predicted participants' behavioral performance.

Introduction

The world surrounding us is inherently multisensory and requires continuous processing and accurate combination of information from the different sensory systems. Constantly, multisensory interactions occur in the brain to evaluate agreement or conflict of different sensory signals. Crossmodal interplay has been shown to impact perception (1) as well as a broad range of cognitive processes (2-4). Thus, flexible interactions of spatially distributed and functionally specialized sensory and other areas of the brain are fundamental to perception, cognition and action. Yet, the neurophysiological implementation of these interactions remains a subject of active exploration. It has been proposed that synchronization of oscillatory signals might subserve the dynamic formation of task-dependent cortical networks (5-9). Only recently, transient synchronization of neuronal signals has also been implicated in establishing relationships across different sensory systems (10, 11), allowing the preferential routing of matching crossmodal information to downstream assemblies (12). There is growing evidence relating multisensory processing to changes in oscillatory power (12-17). In contrast, only few studies have explicitly assessed phase dynamics of multiple brain signals in the context of crossmodal interaction. Experimental evidence directly linking neural coherence and multimodal processing comes from invasive recordings in behaving animals (18-20) as well as a small number of studies in humans performed with EEG and MEG (21-24).

In the current study, we sought to investigate global patterns of long-range synchronization in distributed cortical networks as observed in multisensory processing. To this end, we used a crossmodal matching paradigm requiring the identification of concurrently presented visual and tactile dot patterns in combination

with high-density EEG recordings. In a similar previous study (25), we found that congruent as compared to incongruent visual-tactile stimulation reliably led to improved behavioral performance in a crossmodal detection task. Here, we aimed at characterizing the neurophysiological correlates of these congruence effects by mapping the involved multisensory networks in space, time and frequency, employing an approach for data-driven analysis of coupling in source space that has recently been developed by our group (26). We investigated whether coherence of oscillatory signals across cortical regions is crucial for the perception and integration of multimodal information. Critically, we tested for the functional relevance of the synchronized networks observed in visual-tactile pattern matching by relating large-scale neural coherence to crossmodal stimulus congruence and participants' task performance.

Results

Behavioral performance

In this study, participants (n = 16) performed a bimodal target detection task, with high-density EEG being recorded simultaneously. The target was one of four spatial dot patterns (Figure 1A), which was introduced at the beginning of each experimental block in both visual (left visual field) and tactile (right finger) modalities. In each trial, different combinations of patterns – that could either be congruent or incongruent – were concurrently delivered in the two modalities and participants were instructed to detect the predefined target in either of them. This yielded four stimulus types: (1) only the tactile stimulus matched the target (T, 16.7%); (2) only the visual stimulus matched the target (V, 16.7%); (3) visual and tactile patterns matched the target (VT, 16.7%); and (4) none of the two patterns matched the target stimulus (50%). In our analysis, we focused on correctly detected (T, V and VT) targets. Trial timing is depicted in Figure 1B.

Repeated-measures ANOVAs comparing accuracy and reaction time data for the different target cases revealed significant differences related to crossmodal stimulus congruence ($F_{2, 14} = 23.28$, $p < 0.0001$ for accuracies; and $F_{2, 14} = 6.59$, $p < 0.01$ for reaction times) with congruent VT targets being associated with the best performance, followed by V and T targets in both accuracy and reaction time. Detailed analyses of the behavioral and oscillatory power data are reported elsewhere (27).

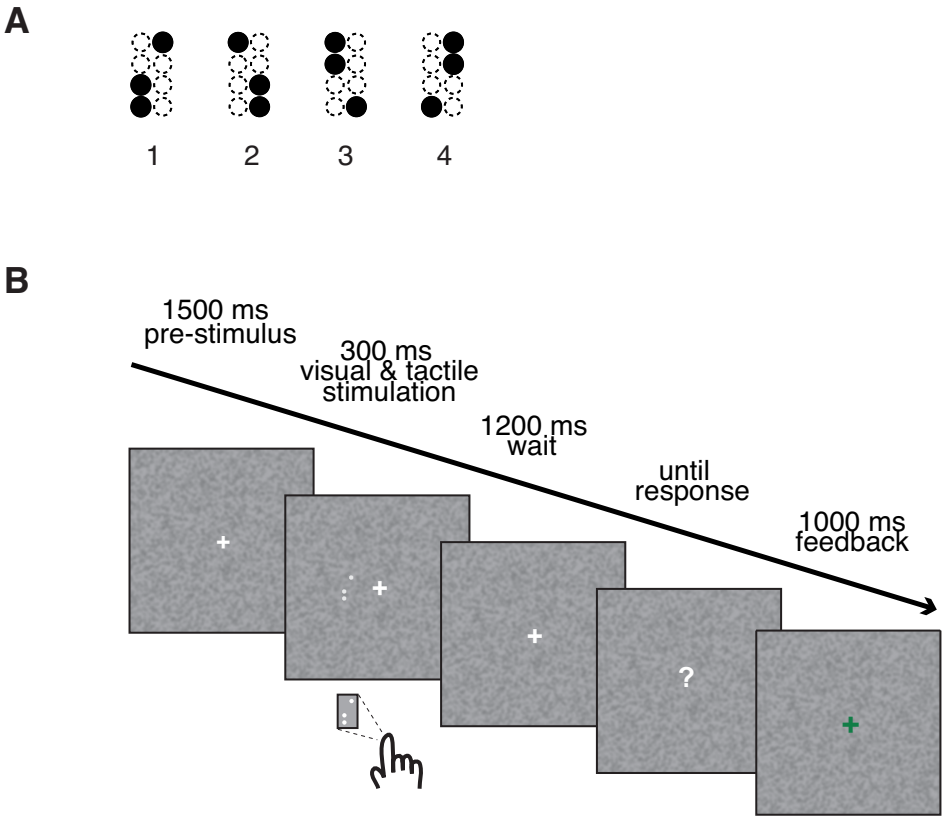

Figure 1. Schematic representation of the visual-tactile detection task. (**A**) The four pattern stimuli used in our experiment. (**B**) The trial sequence. After a pre-stimulus interval of 1500 ms, visual and tactile stimuli were presented simultaneously for 300 ms, followed by a wait interval of 1200 ms. After that, a question mark appeared on the screen indicating that responses could be given. After button press, visual feedback was given (1000 ms).

Identifying networks of remote cortical synchronization

In this study, we focus on analyzing the coordination of brain activity among remote areas. We adopted a recently published purely data-driven method (26) to identify brain networks formed by cortical synchronization. Time-frequency decomposition of the EEG sensor data was performed using the multi-taper approach (28). Afterwards, the full spectrum including all time and frequency bins was projected to source space using beamforming (29). Since we did not want to constrain our analysis by a priori assumptions concerning the location of the networks involved in the crossmodal task, we constructed the source space as 324 evenly distributed voxels covering the whole

cortex. We chose coherence (30) to measure neural coupling in source space, which was applied to all locations pairs. Further, instead of investigating the directly measured values, we compared coupling measures between well-controlled conditions. This was done to avoid possible spatial synchronization patterns caused by irrelevant sources common to all conditions (e.g. heart beats). The difference in coherence was submitted to spatial filtering and then clustered in multi-dimensional space with locations, time and frequency. To account for the problem of multiple comparisons (see *Methods* section for details), permutation statistics (31) was performed to identify the synchronized networks. This method enabled us to investigate interactions between remote brain areas without any a priori assumptions about the time, frequency, size, location, number or structure of the involved networks.

One beta network involved in target detection

First, we applied the network identification approach to the difference in coherence between stimulation and baseline activity. A highly structured network associated with target detection was identified (permutation-test, $p < 0.001$, cluster 1, Figure 2), exhibiting stronger beta (~ 20 Hz) synchronization compared to baseline, which started around 600 ms, and peaked at 800 ms after stimulus onset (Figure 2B). The most strongly connected region in this network was intraparietal sulcus (IPS), accounting for 5268 of 13641 total connections, a large proportion of which (4945) were long-range connections to other areas, including the primary somatosensory cortex (S1), supramarginal gyrus (SMG), primary motor cortex (M1) and premotor cortex (PM, Figure 2A, Figure S1A). The left-hemispheric distribution of the network was in line with the location of tactile stimulation (right index finger), suggesting this

network was related to sensory information processing. The involvement of IPS suggests a similarity to findings reported previously on visual-auditory integration during bi-stable perception (26). This finding was also consistent with the hypothesis

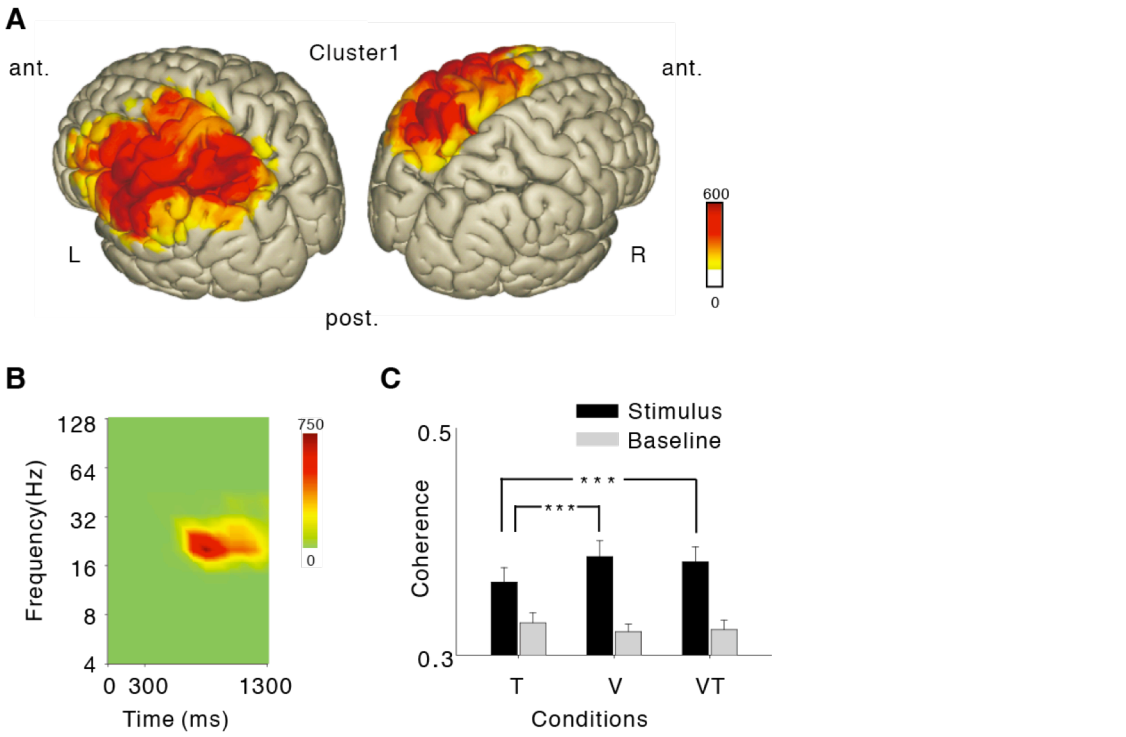

Figure 2: Beta synchrony network related to the detection task. (**A**) Spatial localization of cortical areas involved in the network. At each location, the color indicates how many connections were stronger after stimulation than baseline, between this location and all other locations, in all time and frequency bins. (**B**) Spectro-temporal coherence profile of the network, showing between how many locations coherence was increased at a given time and frequency point compared with baseline. (**C**) Comparison of coherence for three conditions: T, V and VT. Black bars represent coherence values for the stimulus interval and gray bars are for baseline. Error bars represent standard errors (N = 16). *** $p<0.001$. There are significant differences between stimulus and baseline for all 3 conditions.

that parietal cortex constitutes a prominent hub in the human brain, as supported by both anatomical and functional studies on resting state connectivity (32).

Compared to the overall distribution of coherence values, those of cluster 1 were more pronounced (Figure S2). Follow-up analyses were conducted to test whether synchronization within the network differed between stimulus conditions. We

performed a repeated-measures ANOVA with two factors: stimulus condition (T, V and VT) and brain state (stimulus vs. baseline). A significant interaction ($F_{2,14}$ = 13.592, p = 0.001), as well as significant main effects were observed. Of course, we expected the contrast for stimulus vs. baseline ($F_{1,15}$ = 33.117, p < 0.0001) to be significant, as the cluster itself was identified based on that comparison. Next, we performed post-hoc analysis to examine differences in coupling related to crossmodal stimulus congruence. We found significant differences between the three stimulus conditions in the time window of interest ($F_{2,14}$ = 15.094, p < 0.001) but not in the baseline interval ($F_{2,14}$ = 1.967, p = 0.177). This indicated that coupling changed in response to different crossmodal stimulus configurations, but was not different for the baseline period. Pairwise examination showed that the overall within-network coherence was stronger in the congruent VT condition than the T condition (paired t-test, p < 0.0001); and stronger in the V condition than the T condition as well (paired t-test, p < 0.0001).

Two beta networks that differ between conditions

We also applied our network identification approach to the difference between conditions, i.e., we contrasted connections between the VT and the V condition (VT – V), and between the VT and the T condition (VT – T). Two networks (cluster 2 and 3, Figure 3) were observed for the latter comparison.

Cluster 2 (permutation test, p = 0.017) involved the following brain areas: IPS, S1, PM, M1, and SMG, all located in the left hemisphere (Figure 3A, Figure S1B). IPS was most (106 of 219) connected, and all of its connections were long-range. As can be seen in Figure 3B, cluster 2 started to evolve around 600 ms and peaked at 700 ms

after stimulus onset. Its frequency was around 20 Hz (Figure 3B). Characteristics of the second cluster were similar to the first one, but spatially and temporally a bit more specific. Baseline coherence, as measured for the frequency and spatial distribution of this cluster, did not differ between condition VT and T ($t_{1, 15} = 1.358$, $p = 0.195$). This suggested that the condition difference in this cluster was not caused by variations in

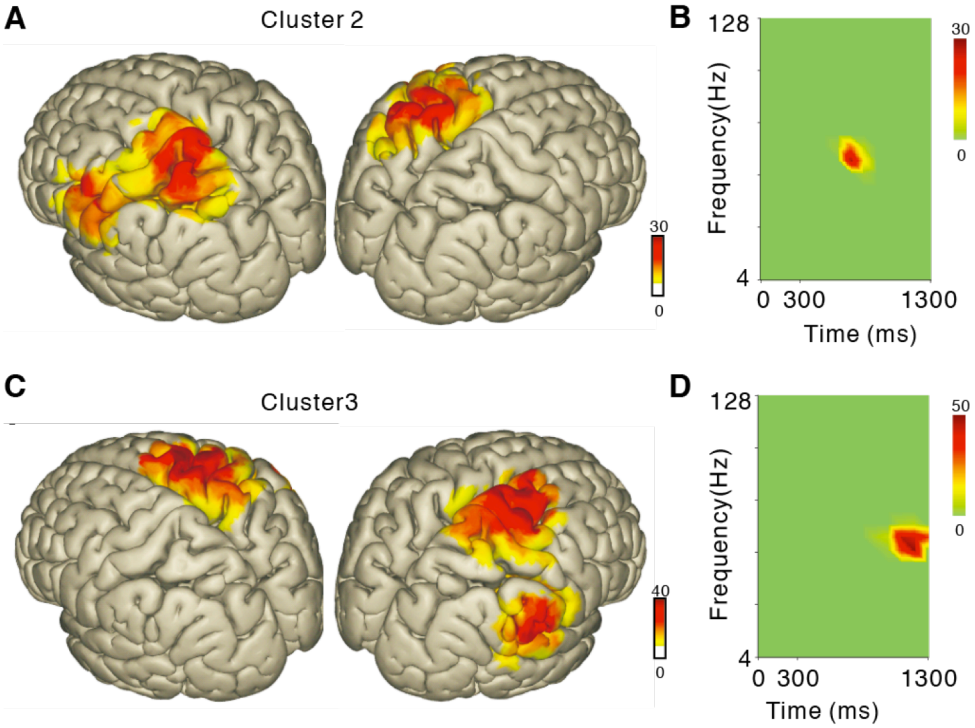

Figure 3. Two beta synchrony networks showing differences between VT and T conditions. (**A**) Spatial localization of cortical clusters showing coherence differences between VT and T conditions. In each location, the color indicates how many connections are stronger in the VT condition than the T condition only, between this location and all other locations, in all time and frequency bins. (**B**) Spectro-temporal coherence profile of the network, showing the number of locations with increased coherence at a given time and frequency bin. (**C-D**) are similar to (**A-B**) but for the third cluster.

baseline connectivity.

Cluster 3 (permutation test, $p = 0.010$) was distinct from the other two. It mainly distributed in the right hemisphere (Figure 3C, Figure S1C), including brain areas SMG, M1, S1, and supplementary motor area (SMA). The most strongly connected

region in this cluster was SMG (196 of 277), and all of its connections were remote. The key role of SMG in visual-tactile integration is consistent with a recent study (33). Coupling in this network emerged around 900 ms and peaked at 1200 ms after stimulus onset (Figure 3D). The relatively late engagement and the lateralization of this cluster (right hemisphere, the response hand was left) suggest that this network may be related to processes of response preparation and execution. Again, we compared coherence between the VT and the T condition also in the baseline period, which yielded no significance ($t_{1,\,15} = 0.927$, $p = 0.369$).

Synchrony within the networks was correlated with performance

In addition to the analysis of long-range coupling, we also tested for local power effects in the involved brain areas at the corresponding time and frequency. We found significant power differences between conditions in all three networks, with power being stronger for VT and V compared to the T condition (Figure 4A). To make sure that the observed connectivity differences represent genuine changes in coupling rather than consequences of power-related variations in signal to noise ratios, we conducted additional analyses and related behavioral performance to specific coupling features. For each subject, we first took the average phase angle of all correct trials for each connection as the optimal angle. Subsequently, for each trial and connection we computed the phase delay to the optimal angle and then averaged across all connections as an index of how close this trial was to an optimal coupling state. Then all trials (including wrong trials) were split into two groups with identical sizes, one with smaller delay to the optimal phase and the other with larger delay. The performance of each group was calculated and statistical analysis was performed

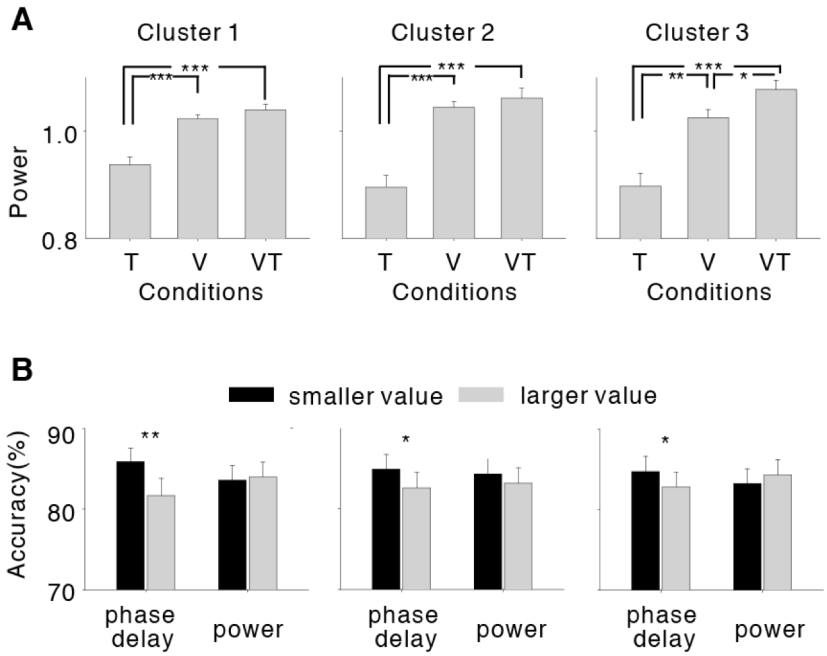

Figure 4. Examination of power confounds and behavioral relevance of long-range coupling. (**A**) Comparison of local power change in brain areas involved in the three beta-band networks. Power values were normalized to the mean of each subject. (**B**) Comparison of performance with trials being either grouped by phase delay to average phase, or power strength; black bars represent smaller and gray bars represent larger phase delays, or differences to average power, respectively. Error bars represent standard errors (N = 16). * - $p< 0.05$, ** - $p< 0.01$, *** - $p <0.001$.

across subjects. For all clusters, the group with smaller phase delay to the optimal state had higher accuracy (Figure 4B). Similarly, we split trials according to power values and related them to behavioral performance. We found no significant difference between the larger power and smaller power groups in any of the 3 clusters. This suggested that phase coupling within the observed networks effectively facilitated performance on the task, which could not be explained by power effects.

Discussion

In the current study, we applied a set of purely data-driven methods for the analysis of complex brain dynamics to high-density EEG recordings from a multisensory paradigm. Throughout the experiment, participants were presented with bimodal visual-tactile stimulation and were instructed to detect predefined target patterns that could appear in either of the two modalities. Three clusters of interacting sources were identified, which showed task- and condition-specific coherence effects in the beta frequency range. Further, the coupling phases within these networks were correlated with the subjects' behavioral performance.

Synchronous beta-band networks for multisensory detection

Our results strongly support the claim that neural synchronization is vital to long-range coordination in the brain, facilitating perceptual organization of sensory information and sensorimotor integration. This adds to growing evidence showing that large-scale cortical synchronization plays an important role in various cognitive functions, including selective attention (34, 35), learning (36), and cross-modal integration (19). The networks observed in the current study synchronized their activity in the beta-band, suggesting central importance of these frequencies for the interaction between remote brain areas (37). This is in line with predictions from computational modeling (38, 39), evidence from invasive recordings in monkeys (34, 40, 41), and clinical studies in different patient groups (42-44).

The networks identified as cluster 1 and cluster 2 in our study (Figure 2, Figure 3 A, B) are likely to be one network obtained with two different procedures. Coupling within this network was enhanced for the condition where crossmodal information was congruently matching the target stimulus (VT), compared to the incongruent case where only the tactile pattern matched the target (T). This could be interpreted in terms of the recent hypothesis that beta-band synchronization is more pronounced for the maintenance of the current status (45). In the natural environment, humans rely more on vision than the other sensory modalities (46, 47); tactile information is often congruent to the visual input and, thus, provides complementary information (e.g. when we pick apples in the supermarket). In this sense, perceptual experience might have shaped the communication pattern between brain areas to a default pattern of high functional connectivity between multisensory parietal and somatosensory cortices. However, in the T condition of our study, information was conflicting between modalities. In this condition, the usually dominant visual modality was not task-relevant but, rather, processing resources needed to be directed to the tactile modality. This might then require a reduction of functional connectivity with parietal cortex in order to decrease the impact of multisensory top-down influences on somatosensory processing. This line of argument draws upon an analogy to the observation that multimodal signals in parietal cortex are processed in a visually dominated reference frame (48, 49). Thus, in the V condition, although bimodal inputs were also incongruent, solely relying on the usually dominant visual modality was still sufficient to accomplish the task. Thus, the need to deviate from the default interaction pattern may be less critical, which would not yield significant change in beta synchrony compared to the VT condition – as observed in our data.

Whereas the first two clusters likely reflected crossmodal sensory processing, cluster 3 (Figure 3 C, D) might be related to sensorimotor integration, decision making and response preparation. Similar to cluster 2, synchronization was stronger for the VT condition as compared to the T condition. Again, reduced beta coherence for the T condition could signal the deviation from the default state of multisensory congruence. Timing and spatial distribution of the third cluster are compatible with recent studies (50, 51), which have linked beta-band activity to decision making in visual motion detection.

Computational modeling (39, 52) suggests that top-down processing in beta network functions can be maintained in the absence of sensory input and may involve modulation of inhibitory interneurons in the target area. The results of our study seem to agree with these proposals showing that beta-band synchronization between parietal and somatosensory cortex decreased when tactile information was needed to successfully perform on the task – possibly leading to a reduction of inhibition. Similar findings were reported in monkey studies (34, 53, 54). The mechanism could be that, as an adaption to regular input patterns, default beta-band networks are established through long-range inhibition across brain areas, facilitating sensory processing, sensorimotor integration and ultimately performance. Whenever deviations from constellations predicted as most likely occur (e.g. conflicting crossmodal stimulation is detected), beta-band coupling decreases to recalibrate performance.

Methodology and critique

In this study, we applied a recently published data-driven method for the identification of long-range networks of cortical synchronization (26). To our best knowledge, this is the first study investigating source space connectivity in a setting requiring multisensory interaction in a purely data-driven way. In general, statistical examination of experimental effects can prevent us from biasing results in favor of a priori hypotheses. However, it cannot correct the bias of data pre-selection with regards to time, space or frequency. The methodology employed in the current study allowed exploring neuronal dynamics in source space covering most of the cortex with a wide range of time and frequency being examined. This provided a quite objective evaluation of our data without a priori constraints.

However, this method has its limitations, too. Investigating a multi-dimensional space, it has to account for a massive multiple-comparison problem, making it less sensitive. It is therefore possible that networks involved in early interaction between sensory areas (i.e. between visual and tactile areas), failed to be identified with our approach. Another limitation of this high-dimensional data space is that in order to avoid extensive computational effort we used a relatively coarse resolution for analysis in source space. However, it was compatible with our anatomical data, i.e., template MRIs and averaged sensor locations.

In this study, only coherence between location pairs in the same frequency range was considered. For future studies, it would be promising to include cross-frequency coupling as well. For example, it would be of interest to investigate the relation of beta phase and gamma power, and its modulation depending on crossmodal congruence.

Importantly, in addition to the data-driven methods, we employed a phase analysis approach inspired by invasive studies (9). By directly relating coupling features, i.e., phase angle, to behavior we showed that neural coherence within the observed multisensory networks effectively facilitated performance on the task.

Power and coupling

Analyses of the behavioral effects and oscillatory power in the same dataset are detailed elsewhere (27). Summing up, we found power differences related to visual-tactile stimulus congruence in the theta- (2-7 Hz), alpha- (8-13 Hz) and beta-band (13-25 Hz). We positioned these findings within a recent framework suggesting that integrative functions involving long-range interactions are predominantly mediated by lower frequencies(20, 55) and proposed that the observed differences in oscillatory dynamics might relate to distinct subcomponents of multisensory integration, such as multisensory gating and crossmodal perceptual decision making. Here, we extend these findings by explicitly assessing phase dynamics of multiple brain signals and mapping the multisensory networks mediating visual-tactile integration in space, time and frequency. Unlike previous work (26), we did not observe a dissociation between local oscillatory activity and long-range synchronization but in contrast found parallel condition differences in power and coherence in the beta-band. However, our additional analysis minimized the risk that the observed coupling patterns were trivial effects of power differences: phase delays calculated on single trial basis were predictive of behavioral performance – in contrast to power. Thus, coupling within the observed networks effectively facilitated performance on the task. These results support the notion that local activation as measured with oscillatory power and remote coupling are complementary to each other in multi-modal tasks.

Summary

In the current study, we provide evidence for a functional role of beta-band coherence in integrating distributed information in multisensory networks. Our data suggest that functional networks defined by beta-band synchrony may be involved in crossmodal sensory processing as well as decision-related processes. Additionally, we demonstrated the functional relevance of inter-areal synchronization for behavior by directly relating phase dynamics to task performance.

Materials and Methods

Participants

Sixteen right-handed volunteers (12 female, mean age 25.4, range 21-33) participated in the current experiment and were compensated in monetary form. Participants had normal or corrected to normal vision and reported no history of neurological or psychiatric illness. The study was approved by the Ethics Committee of the Medical Association Hamburg and conducted in accordance with the Declaration of Helsinki. Prior to the recordings, all participants provided written informed consent.

Task design

In the current experiment, we employed a setup similar to the one realized in a previous behavioral study (25). Figure 1 provides an overview of events and timing of the visual-tactile matching paradigm used here. The stimulus set consisted of four spatial patterns, each of them formed by three dots (Figure 1A). Stimulation was always bimodal, with visual and tactile patterns being presented concurrently on a computer screen and to participants' index fingertip via a Braille stimulator (QuaeroSys Medical Devices, Schotten, Germany). Visual stimuli appeared left of a central fixation cross and were embedded in a noisy background while tactile patterns were delivered to the right index finger. Stimulus duration was 300 ms for both patterns.

To familiarize participants with the tactile stimuli, we conducted a delayed-match-to-sample training task prior to the actual experiment (for details see (27)). One participant was excluded after the training procedure due to insufficient performance.

Participants were instructed to detect predefined target stimuli that could appear in both modalities. At the beginning of each experimental block, one of the four patterns was defined as the target stimulus (the other three patterns were non-targets, respectively) by simultaneously presenting it on the computer screen and by means of the Braille stimulator (four times). During the experimental block, the target could appear in the visual or the tactile modality alone, in both or in neither of the two. Participants were asked to decide whether the presented stimuli matched the previously defined target or not and press one of two response buttons accordingly. Participants responded with their left hand via button press on a response box (Cedrus, RB-420 Model, San Pedro, USA) and visual feedback (a green '+' or a red '–') was given in every trial. The timing of events is displayed in Figure 1B.

In two sessions happening within three days, we recorded 1536 trials from each participant. The design was counterbalanced with respect to crossmodal stimulus congruence, target definition and presentation frequency of each of the four patterns (for details see (25)). Data from the two recording sessions were pooled and trials grouped according to target appearance, resulting in the following conditions: tactile-matching only (a tactile target presented with a visual non-target; labeled as T), visual-matching only (a visual target appearing with a tactile non-target; V), and visual-tactile targets (VT) as well as non-target congruent or incongruent pairs. In our cluster identification analysis, we focused on correctly detected (V, T and VT) trials. For each of these conditions, 192 trials were presented across the two recording sessions.

Key mapping (for 'target' and 'non-target'-buttons) was counterbalanced across participants and sessions. Sounds associated with pin movement in the Braille cells were masked with pink noise administered via foam-protected air tube earphones at

75 dB sound pressure level (Eartone, EAR Auditory Systems, AearoCompany). We used Presentation software (Neurobehavioral Systems, version 16.3) to control stimulus presentation and to record participants' response times (RT) and accuracies.

EEG data collection and preprocessing

Electroencephalographic data were acquired from 126 scalp sites using Ag/AgCl ring electrodes mounted into an elastic cap (EASYCAP, Herrsching, Germany). Two additional electrodes were placed below the eyes to record the electrooculogram. EEG data were recorded with a passband of 0.016-250 Hz and digitized with a sampling rate of 1000 Hz using BrainAmp amplifiers (BrainProducts, Munich, Germany). During the recordings, the tip of the nose served as a reference but subsequently we re-referenced the data to common average. Preprocessing of the EEG data was carried out in Matlab 8.0 (MathWorks, Natick, MA) using custom-made scripts, as well as routines incorporated in EEGLAB 11.0 ((56); http://sccn.ucsd.edu/eeglab/). Offline, the data were band-pass filtered (0.3-180 Hz), downsampled to 500 Hz and epoched from – 400 to + 1400 ms around stimulus onset. Next, all trials were inspected visually and those containing EMG artifacts were rejected. To remove artifacts related to eyeblinks, horizontal eye movements and electrocardiographic activity, we applied an independent component analysis (ICA) approach. Furthermore, we employed the COSTRAP algorithm (correction of saccade-related transient potentials; (57)) to control for miniature saccadic artifacts. This algorithm has been used in previous studies (e.g. (58, 59)) to suppress ocular sources of high frequency signals. Employing this multilevel artifact correction procedure, 88% of all recorded trials (range: 75% to 95% for individual participants) were retained. The number of trials

for all three conditions was stratified before applying the cluster identification approach based on differences between conditions.

EEG time-frequency decomposition

All spectral estimates were performed using the multitaper method (28, 60). Spectral estimates were computed across 21 logarithmically scaled frequencies from 4 to 128 Hz with 0.25 octave steps; and across 17 time points from -300 to 1300 ms in 100 ms steps. The temporal and spectral smoothing was performed as follows. For frequencies larger or equal to 16 Hz, we used temporal windows of 250 ms and adjusted the number of slepian tapers to approximate a spectral smoothing of 3/4 octave; for frequencies lower than 16 Hz, we adjusted the time window to yield a frequency smoothing of 3/4 octaves with a single taper (26). In case the window extended outside of the full data range (-400 – 1400 ms), zeros were padded. We characterized power and coherence responses relative to the prestimulus baseline using the bin at -200 ms. The employed time frequency transformation ensured a homogenous sampling and smoothing in time and frequency, as required for subsequent clustering within this space.

Source estimation of frequency-specific activity

We first constructed our source space based on the template brain ICBM152 from the Montreal Neurological Institute (61). The cortex was segmented using freesurfer software (62, 63). After that, we employed the MNE software package (64) to define our source space as 324 locations homogeneously covering the whole cortex. Then, we computed leadfields with these source locations, and averaged sensor locations from ~ 30 subjects whose data were registered in previous studies in our laboratory.

Leadfield calculation was realized as described in a previous paper (65) with a 3-shell head model based on the same brain template. We used the beamforming method (29) to estimate the spectral amplitude and phase of neural population signals at the cortical source level. For each time point, frequency, and source location, we computed three orthogonal filters (one for each spatial dimension) that passed activity from the location of interest with unit gain, while maximally suppressing activity from all other sources. We then linearly combined the three filters into a single filter in the direction of maximal variance (26). To derive the complex source estimates, we multiplied the complex frequency domain data with the real-valued filter. We used all data trials to compute the filter common to all conditions in order to avoid spurious effects resulting from unequal filters. It should be noted that high source correlations can reduce source amplitudes estimated with beamforming due to source cancelation (66). This may, in turn, affect the magnitude of cortico-cortical coherence estimates. However, within the range of physiological source-correlations (67), this does not prevent the identification of cortico-cortical coherence using beamforming (68). Moreover, although source-cancelation may affect the magnitude of, and reduce the sensitivity to detect coherence, it may not lead to false positive results.

Coupling analysis

We estimated coherence to quantify the frequency-dependent synchronization between pairs of signals $X(f, t)$ and $Y(f, t)$ according to the following equation:

$$C_{xy}(f,t) = \frac{\sum_i X(f,t)\, Y^*(f,t)}{\sqrt{(\sum_i X(f,t)X^*(f,t))(\sum_i Y(f,t)Y^*(f,t))}} \quad (1)$$

Since coherence is positively biased to 1 with decreasing number of independent spectral estimates (degrees of freedom), we stratified the sample size and used the

same number of trials for the comparison between conditions. We also performed a nonlinear transform (69) to render the coherence distribution to approximately Gaussian before clustering with the following equation:

$$C_z = \beta(q - \beta), \quad q = \sqrt{-(v-2)\log(1-|C|^2)} \qquad (2)$$

Here β is a constant 23/20; v is the degree of freedom; C is coherence.

Identification of Synchronized Networks

The general approach of our network identification followed the method described in a previous study (26), which is summarized below. An interaction between two cortical areas could be extended from a point in a two-dimensional space to that in a four-dimensional space when time and frequency were involved. Thus, identifying networks of significant interaction would be equivalent to identifying continuous clusters within this high-dimensional space. In our approach, we first computed coherences for all pairs of locations in all time and frequency bins and conditions with equation (1), which were later transformed with equation (2) to be Gaussian. Then *t*-statistics was performed across subjects, contrasting either between data after stimulus onset to baseline in all trials, or between data of condition pair VT *vs.* V or VT *vs.* V with stratified trial numbers. The 4-D (location by location by frequency by time) matrix was then thresholded with a *t*-value equivalent to $p < 0.01$ to be 1 (connected) or 0 (not connected). Further, the resulting matrix was spatially filtered by a threshold of 0.5 to remove spurious connections, i.e. if the average neighboring connection value of a connection was less than 0.5, this connection would be set to 0. This procedure removed spurious bridges between connection clusters. Then the remaining networks linked by direct neighbor connections were identified as clusters, which

corresponded to networks of cortical regions with different synchronization status among comparisons, and were continuous across time, frequency, and pairwise space. We defined their sizes as the integral of the *t*-scores across the volume of the cluster. To evaluate their significance, random permutation statistics was performed to account for multiple comparisons across the interaction space; i.e. the network-identification approach was repeated 2000 times with shuffled condition labels to create an empirical distribution of cluster sizes under the null-hypothesis of no difference between conditions (31). The null-distribution was constructed from the largest clusters (two-tailed) of each resample, and only clusters with sizes ranked top 5% in these null distributions were considered as significant.

Illustration of identified networks

To visualize the identified networks, we projected them onto two subspaces separately. We computed for each location the integral of the corresponding cluster in the connection space over time, frequency, and target locations. The result was then displayed on the template brain surface and revealed the spatial extent of the network independent of its intrinsic synchronization structure and location in time and frequency. Complementary to this, we integrated the connections over all spatial locations for each time and frequency bin to illustrate when and at which frequencies a cluster was active irrespective of the spatial distribution.

Further analyses of identified networks

To analyze the spatial patterns within the observed clusters, we defined several regions of interest (ROIs) according to a cortex-based atlas (70, 71). The connections

from each ROI were summed as an index of how much this ROI was involved in the network. To analyze further properties of the network identified by coherence differences between stimulus and baseline, we averaged coherence values across all location pairs, times and frequencies for the three conditions separately, and their corresponding values in baseline as well. These data for all subjects were submitted to a 3 x 2 repeated-measures ANOVA, with two within-subject factors: stimulus condition (VT, V and T) and brain state (stimulus and baseline). Post-hoc analysis was performed for simple effects. The aggregated power of each cluster was also compared in a similar manner to check whether the local changes were correlated with the remote ones. To test further the independency of the latter, we classified the trials according to the phase relations, inspired by previous work in monkeys (9). The average phase angle across all correct trials, for each pair of locations in a certain time and frequency was taken as the optimal phase angle. For each trial, we measured the deviation of the phase angles from this optimal one and averaged across all location pairs, times and frequencies, as an index of how close this trial was to the optimal coupling state. Then, for each subject, trials were classified into two groups with identical trial numbers, one with smaller phase delay from the optimal and the other with lager phase delay, irrespective of stimulus type. To test whether the phase delay was functionally relevant for behavior, performance in either group was compared across subjects. A similar approach was performed for the power data at the locations/times/frequencies involved in the network of interest.

Acknowledgments

This research was supported by grants from the German Research Foundation (SFB 936/A3/B6) and the European Union (ERC-2010-AdG-269716) awarded to A.K.E. and P.K. The authors thank Guido Nolte, Jörg Hipp and Till Schneider for methodological support, Jonathan Daume for constructive discussions and Julia Diestel for assistance in data recording.

Author contributions: F.G., U.F., P.K. and A.K.E. designed research; F.G. performed research; P.W. and F.G. analyzed data; P.W., F.G. and A. K. E. wrote the paper; P.W., F.G., U.F., P.K. and A.K.E. discussed the results, edited and approved the manuscript.

References

1. McGurk H & MacDonald J (1976) Hearing lips and seeing voices. *Nature* 264(5588):746-748.
2. Stein BE (2012) *The new handbook of multisensory processing* (MIT Press, Cambridge, Mass.) 824 p.
3. Macaluso E & Driver J (2005) Multisensory spatial interactions: a window onto functional integration in the human brain. *Trends Neurosci* 28(5):264-271.
4. Driver J & Spence C (2000) Multisensory perception: beyond modularity and convergence. *Curr Biol* 10(20):R731-735.
5. Engel AK, Fries P, & Singer W (2001) Dynamic predictions: oscillations and synchrony in top-down processing. *Nat. Rev. Neurosci.* 2(10):704-716.
6. Fries P (2005) A mechanism for cognitive dynamics: neuronal communication through neuronal coherence. *Trends Cogn Sci* 9(10):474-480.
7. Salinas E & Sejnowski TJ (2001) Correlated neuronal activity and the flow of neural information. *Nat. Rev. Neurosci.* 2(8):539-550.
8. Varela F, Lachaux JP, Rodriguez E, & Martinerie J (2001) The brainweb: phase synchronization and large-scale integration. *Nat Rev Neurosci* 2(4):229-239.
9. Womelsdorf T*, et al.* (2007) Modulation of neuronal interactions through neuronal synchronization. *Science* 316(5831):1609-1612.
10. Lakatos P, Chen CM, O'Connell MN, Mills A, & Schroeder CE (2007) Neuronal oscillations and multisensory interaction in primary auditory cortex. *Neuron* 53(2):279-292.
11. Kayser C, Petkov CI, & Logothetis NK (2008) Visual modulation of neurons in auditory cortex. *Cereb Cortex* 18(7):1560-1574.
12. Senkowski D, Schneider TR, Foxe JJ, & Engel AK (2008) Crossmodal binding through neural coherence: implications for multisensory processing. *Trends Neurosci* 31(8):401-409.
13. Bauer M, Oostenveld R, & Fries P (2009) Tactile stimulation accelerates behavioral responses to visual stimuli through enhancement of occipital gamma-band activity. *Vision Res* 49(9):931-942.
14. Schneider TR, Debener S, Oostenveld R, & Engel AK (2008) Enhanced EEG gamma-band activity reflects multisensory semantic matching in visual-to-auditory object priming. *Neuroimage* 42(3):1244-1254.
15. Schneider TR, Lorenz S, Senkowski D, & Engel AK (2011) Gamma-band activity as a signature for cross-modal priming of auditory object recognition by active haptic exploration. *J Neurosci* 31(7):2502-2510.
16. Gleiss S & Kayser C (2014) Oscillatory mechanisms underlying the enhancement of visual motion perception by multisensory congruency. *Neuropsychologia* 53:84-93.
17. Senkowski D, Pomper U, Fitzner I, Engel AK, & Kral A (2014) Beta-band activity in auditory pathways reflects speech localization and recognition in bilateral cochlear implant users. *Hum Brain Mapp* 35(7):3107-3121.
18. Kayser C & Logothetis NK (2009) Directed interactions between auditory and superior temporal cortices and their role in sensory integration. *Front Integr Neurosci* 3:7.
19. Maier JX, Chandrasekaran C, & Ghazanfar AA (2008) Integration of bimodal looming signals through neuronal coherence in the temporal lobe. *Curr Biol* 18(13):963-968.
20. von Stein A, Chiang C, & Konig P (2000) Top-down processing mediated by interareal synchronization. *Proc Natl Acad Sci USA* 97(26):14748-14753.

21. Doesburg SM, Emberson LL, Rahi A, Cameron D, & Ward LM (2008) Asynchrony from synchrony: long-range gamma-band neural synchrony accompanies perception of audiovisual speech asynchrony. *Exp Brain Res* 185(1):11-20.
22. Hummel F & Gerloff C (2005) Larger interregional synchrony is associated with greater behavioral success in a complex sensory integration task in humans. *Cereb Cortex* 15(5):670-678.
23. Lange J, Christian N, & Schnitzler A (2013) Audio-visual congruency alters power and coherence of oscillatory activity within and between cortical areas. *Neuroimage* 79:111-120.
24. van Driel J, Knapen T, van Es DM, & Cohen MX (2014) Interregional alpha-band synchrony supports temporal cross-modal integration. *Neuroimage* 101:404-415.
25. Göschl F, Engel AK, & Friese U (2014) Attention modulates visual-tactile interaction in spatial pattern matching. *PLoS One* 9(9):e106896.
26. Hipp JF, Engel AK, & Siegel M (2011) Oscillatory synchronization in large-scale cortical networks predicts perception. *Neuron* 69(2):387-396.
27. Göschl F, Friese U, Daume J, König P, & Engel AK (2015) Oscillatory signatures of crossmodal congruence effects: An EEG investigation employing a visual-tactile pattern matching paradigm. *bioRxiv. doi : 10.1101/014092*.
28. Mitra PP & Pesaran B (1999) Analysis of dynamic brain imaging data. *Biophys J* 76(2):691-708.
29. Gross J*, et al.* (2001) Dynamic imaging of coherent sources: studying neural interactions in the human brain. *Proc Natl Acad Sci USA* 98(2):694-699.
30. Roach BJ & Mathalon DH (2008) Event-related EEG time-frequency analysis: an overview of measures and an analysis of early gamma band phase locking in schizophrenia. *Schizophr Bull* 34(5):907-926.
31. Nichols TE & Holmes AP (2002) Nonparametric permutation tests for functional neuroimaging: a primer with examples. *Hum Brain Mapp* 15(1):1-25.
32. Bullmore E & Sporns O (2009) Complex brain networks: graph theoretical analysis of structural and functional systems. *Nat Rev Neurosci* 10(3):186-198.
33. Quinn BT*, et al.* (2014) Intracranial cortical responses during visual-tactile integration in humans. *J Neurosci* 34(1):171-181.
34. Buschman TJ & Miller EK (2007) Top-down versus bottom-up control of attention in the prefrontal and posterior parietal cortices. *Science* 315(5820):1860-1862.
35. Siegel M, Donner TH, Oostenveld R, Fries P, & Engel AK (2008) Neuronal synchronization along the dorsal visual pathway reflects the focus of spatial attention. *Neuron* 60(4):709-719.
36. Antzoulatos EG & Miller EK (2014) Increases in functional connectivity between prefrontal cortex and striatum during category learning. *Neuron* 83 (1):216-225.
37. Womelsdorf T & Fries P (2007) The role of neuronal synchronization in selective attention. *Curr Opin Neurobiol* 17(2):154-160.
38. Kopell N, Ermentrout GB, Whittington MA, & Traub RD (2000) Gamma rhythms and beta rhythms have different synchronization properties. *Proc Natl Acad Sci USA* 97(4):1867-1872.
39. Lee JH, Whittington MA, & Kopell NJ (2013) Top-down beta rhythms support selective attention via interlaminar interaction: a model. *PLoS Comput Biol* 9(8):e1003164.
40. Pesaran B, Nelson MJ, & Andersen RA (2008) Free choice activates a decision circuit between frontal and parietal cortex. *Nature* 453(7193):406-U461.
41. Saalmann YB, Pigarev IN, & Vidyasagar TR (2007) Neural mechanisms of visual attention: how top-down feedback highlights relevant locations. *Science* 316(5831):1612-1615.

42. Uhlhaas PJ*, et al.* (2006) Dysfunctional long-range coordination of neural activity during Gestalt perception in schizophrenia. *J Neurosci* 26(31):8168-8175.
43. Bangel KA*, et al.* (2014) Reduced beta band connectivity during number estimation in autism. *NeuroImage Clin* 6:202-213.
44. Leung RC, Ye AX, Wong SM, Taylor MJ, & Doesburg SM (2014) Reduced beta connectivity during emotional face processing in adolescents with autism. *Mol Autism* 5(1):51.
45. Engel AK & Fries P (2010) Beta-band oscillations--signalling the status quo? *Curr Opin Neurobiol* 20(2):156-165.
46. Spence C, Shore DI, & Klein RM (2001) Multisensory prior entry. *J Exp Psychol Gen* 130(4):799-832.
47. Posner MI, Nissen MJ, & Klein RM (1976) Visual dominance: an information-processing account of its origins and significance. *Psychol Rev* 83(2):157-171.
48. Buneo CA, Jarvis MR, Batista AP, & Andersen RA (2002) Direct visuomotor transformations for reaching. *Nature* 416(6881):632-636.
49. Cohen YE & Andersen RA (2002) A common reference frame for movement plans in the posterior parietal cortex. *Nat Rev Neurosci* 3(7):553-562.
50. Donner TH*, et al.* (2007) Population activity in the human dorsal pathway predicts the accuracy of visual motion detection. *J Neurophysiol* 98(1):345-359.
51. Donner TH, Siegel M, Fries P, & Engel AK (2009) Buildup of choice-predictive activity in human motor cortex during perceptual decision making. *Curr Biol* 19(18):1581-1585.
52. Kopell N, Whittington MA, & Kramer MA (2011) Neuronal assembly dynamics in the beta1 frequency range permits short-term memory. *Proc Natl Acad Sci USA* 108(9):3779-3784.
53. Gregoriou GG, Gotts SJ, Zhou H, & Desimone R (2009) High-frequency, long-range coupling between prefrontal and visual cortex during attention. *Science* 324(5931):1207-1210.
54. Buschman TJ & Miller EK (2009) Serial, covert shifts of sttention during visual search are reflected by the frontal eye fields and correlated with population oscillations. *Neuron* 63(3):386-396.
55. Donner TH & Siegel M (2011) A framework for local cortical oscillation patterns. *Trends Cogn Sci* 15(5):191-199.
56. Delorme A & Makeig S (2004) EEGLAB: an open source toolbox for analysis of single-trial EEG dynamics including independent component analysis. *J Neurosci Methods* 134(1):9-21.
57. Hassler U, Barreto NT, & Gruber T (2011) Induced gamma band responses in human EEG after the control of miniature saccadic artifacts. *Neuroimage* 57(4):1411-1421.
58. Hassler U, Friese U, Martens U, Trujillo-Barreto N, & Gruber T (2013) Repetition priming effects dissociate between miniature eye movements and induced gamma-band responses in the human electroencephalogram. *Eur J Neurosci* 38(3):2425-2433.
59. Friese U*, et al.* (2013) Successful memory encoding is associated with increased cross-frequency coupling between frontal theta and posterior gamma oscillations in human scalp-recorded EEG. *Neuroimage* 66:642-647.
60. Thomson DJ (1982) Spectrum estimation and harmonic analysis. *Proceedings of the IEEE* 70(9):1055-1096.
61. Mazziotta JC, Toga AW, Evans A, Fox P, & Lancaster J (1995) A probabilistic atlas of the human brain: theory and rationale for its development. The International Consortium for Brain Mapping (ICBM). *Neuroimage* 2(2):89-101.

62. Dale AM, Fischl B, & Sereno MI (1999) Cortical surface-based analysis. I. Segmentation and surface reconstruction. *Neuroimage* 9(2):179-194.
63. Fischl B, Sereno MI, & Dale AM (1999) Cortical surface-based analysis. II: Inflation, flattening, and a surface-based coordinate system. *Neuroimage* 9(2):195-207.
64. Gramfort A*, et al.* (2014) MNE software for processing MEG and EEG data. *Neuroimage* 86(0):446-460.
65. Nolte G & Dassios G (2005) Analytic expansion of the EEG lead field for realistic volume conductors. *Phys Med Biol* 50(16):3807-3823.
66. Van Veen BD, Van Drongelen W, Yuchtman M, & Suzuki A (1997) Localization of brain electrical activity via linearly constrained minimum variance spatial filtering. *IEEE Trans Biomed Eng* 44(9):867-880.
67. Leopold DA, Murayama Y, & Logothetis NK (2003) Very slow activity fluctuations in monkey visual cortex: implications for functional brain imaging. *Cereb Cortex* 13(4):422-433.
68. Kujala J, Gross J, & Salmelin R (2008) Localization of correlated network activity at the cortical level with MEG. *Neuroimage* 39(4):1706-1720.
69. Jarvis MR & Mitra PP (2001) Sampling properties of the spectrum and coherency of sequences of action potentials. *Neural Comput* 13(4):717-749.
70. Fischl B*, et al.* (2004) Automatically parcellating the human cerebral cortex. *Cereb Cortex* 14(1):11-22.
71. Destrieux C, Fischl B, Dale A, & Halgren E (2010) Automatic parcellation of human cortical gyri and sulci using standard anatomical nomenclature. *Neuroimage* 53(1):1-15.

Supporting information

SI Figures

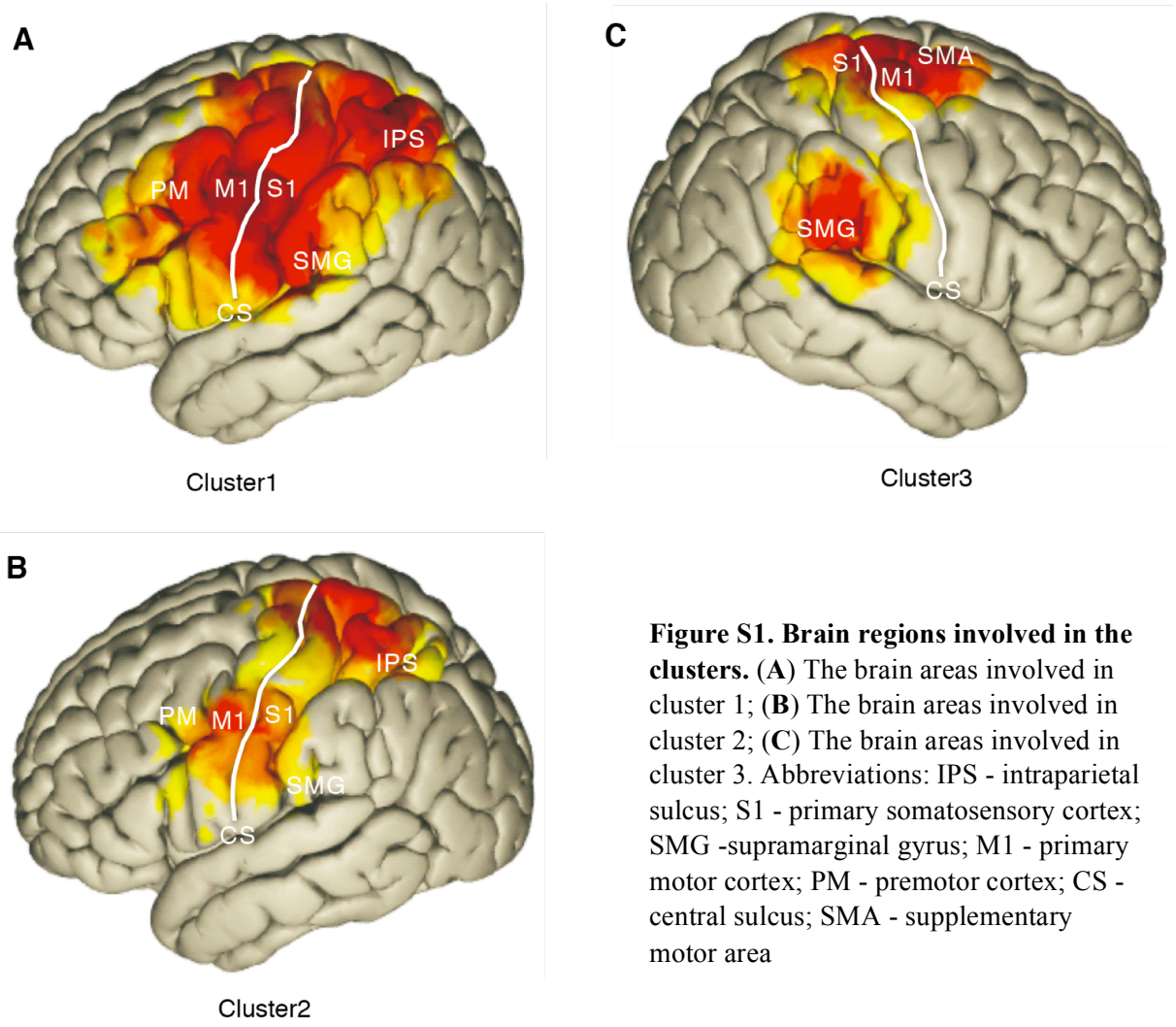

Figure S1. Brain regions involved in the clusters. (**A**) The brain areas involved in cluster 1; (**B**) The brain areas involved in cluster 2; (**C**) The brain areas involved in cluster 3. Abbreviations: IPS - intraparietal sulcus; S1 - primary somatosensory cortex; SMG -supramarginal gyrus; M1 - primary motor cortex; PM - premotor cortex; CS - central sulcus; SMA - supplementary motor area

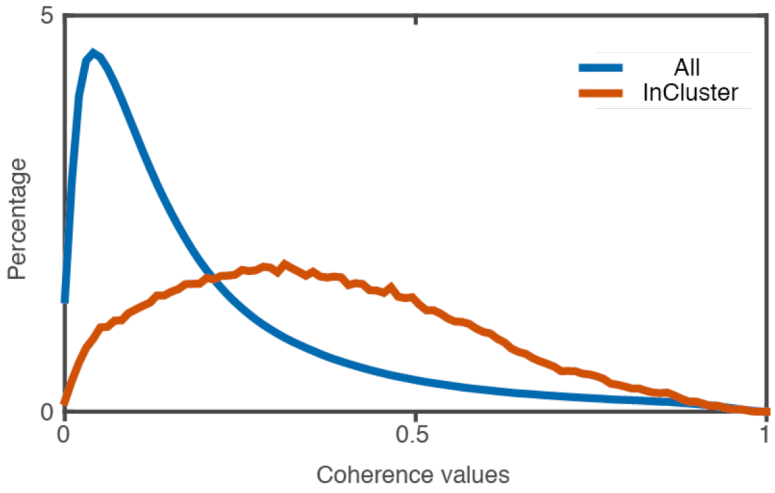

Figure S2. Distribution of coherence values. For this figure, the coherence values were computed on all the trials for all subjects (N = 16). Each curve illustrates the coherence values' distribution in 100 bins, which extends from 0 to 1. The blue curve represents all subjects in all location pairs, time and frequency bins. The orange curve also represents all subjects but only location pairs, time and frequency bins involved in cluster 1. The x-axis is for the bins of coherence values; y-axis is for percentage of overall connections for each bin.